NANO LETTERS

pubs.acs.org/NanoLett Letter

Miniaturizing a Chip-Scale Spectrometer Using Local Strain Engineering and Total-Variation Regularized Reconstruction

Tuba Sarwar, Can Yaras, Xiang Li, Qing Qu, and Pei-Cheng Ku*

Cite This: *Nano Lett.* 2022, 22, 8174−8180 Read Online

ACCESS | Metrics & More | Article Recommendations | Supporting Information

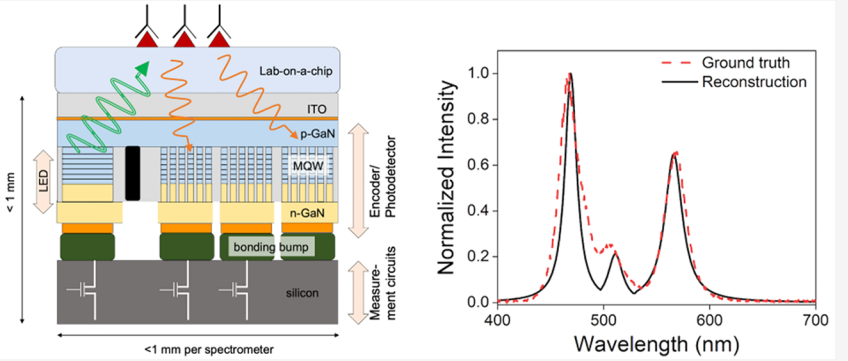

ABSTRACT: A wafer-thin chip-scale portable spectrometer suitable for wearable applications based on a reconstructive algorithm was demonstrated. A total of 16 spectral encoders that simultaneously functioned as photodetectors were monolithically integrated on a chip area of 0.16 mm^2 by applying local strain engineering in compressively strained InGaN/GaN multiple quantum well heterostructures. The built-in GaN pn junction enabled a direct photocurrent measurement. A non-negative least-squares (NNLS) algorithm with total-variation regularization and a choice of a proper kernel function was shown to deliver a decent spectral reconstruction performance in the wavelength range of 400−645 nm. The accuracies of spectral peak positions and intensity ratios between peaks were found to be 0.97% and 10.4%, respectively. No external optics, such as collimation optics and apertures, were used, enabled by angle-insensitive light-harvesting structures, including an array of cone-shaped backreflectors fabricated on the underside of the sapphire substrate.

KEYWORDS: *Gallium nitride, compound semiconductors, photodetection, sapphire, light-emitting diode*

Optical spectroscopy is one of the most important and widely utilized scientific techniques. A spectrometer measures an optical signal's spectrum, that is, the relative spectral power density $P(\lambda)$ at different wavelengths λ. A visible-wavelength spectrometer is a versatile tool for applications in chemistry, life science, microbiology, food industry, biomedical sensing, lab-on-a-chip, environmental monitoring, pharmaceutical research, cosmetic industry, and quality control. A spectroscopic system consists of three parts: a light source for reference or fluorescence excitation, a series of spectral encoders to encode the optical signal from the sample, and one or more photodetectors to convert the encoded signal into the spectrum. The most common Czerny−Turner configuration[1] (e.g., in a monochromator) uses a grating to encode the signal's wavelength onto different spatial coordinates, which are subsequently measured by a linear photodetector array. The Fourier-transform spectrometer (e.g., FTIR) encodes the signal's autocorrelation using a variable delay line that is then converted into the signal's spectrum via the Fourier transform. The tunable light spectrometer (e.g., a tunable laser spectrometer; an oximeter in a smartwatch[2,3]) uses multiple LEDs or a tunable laser as the encoder to isolate the signal one wavelength at a time. However, this approach is unsuitable for detecting an active optical signal from fluorescence, chemi-, and electroluminescence. The reconstructive spectrometer encodes the signal with multiple broadband spectral filters, $R_k(\lambda)$, where k is the index of the spectral encoder.[4] Each of the encoded signals is measured by a separate photodetector. The collective photocurrents $\{I_k\}$ are then used to reconstruct the spectrum, for example, using a non-negative least-squares (NNLS) algorithm $P(\lambda)$:$\min_{P\geq 0}\|I - RP\|^2/2$. The reconstructive spectrometer has attracted intense research interest recently[5,6,15−18,7−14] because of the following: 1. Computational power per watt-dollar grows

Received: July 6, 2022
Revised: October 8, 2022
Published: October 12, 2022

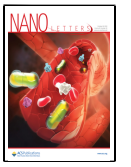

https://doi.org/10.1021/acs.nanolett.2c02654
Nano Lett. 2022, 22, 8174−8180

rapidly; 2. Spectral filters can be highly compact and mass-produced; 3. With machine learning and optimization advances, the spectrum can be efficiently reconstructed even with only a small number of encoders/photodetectors.[17,19,20] These features are especially attractive when miniaturizing a spectroscopic system.

In this Letter, a low-profile reconstructive spectrometer with only the thickness of the semiconductors and an operating range spanning the visible wavelength spectrum is reported. Visible spectrometers have broad applications in UV−vis, fluorescence, and chemi-/electroluminescence spectroscopy. We focus on an extremely portable platform enabled by a total system height including all the necessary optics and electronics of no more than a few hundred microns and an area on the order of 0.1 mm^2. We also favor simple and computationally efficient algorithms. While the spectral resolution and accuracy of our results are limited by the number of detectors that can be fitted in a small chip area, our design can be advantageous for wearable applications that are constrained by size, weight, and power consumption. In this work, the spectral encoders are based on wide-bandgap gallium nitride (GaN) semiconductors and are designed to be as insensitive to the incident angle of light as possible. As GaN semiconductors are excellent light-emitting materials, monolithic integration of a reference or excitation light source on the spectrometer chip is possible and has been shown previously.[21] Heterogeneous integration with a silicon transimpedance amplifier (TIA)[22] or monolithic integration of GaN TIA[23] has also been previously reported for GaN-based detectors.

The GaN-based spectral encoders were programmed using local strain engineering. They had a very weak dependence on the incident angle of light,[14] eliminating the need to condition the optical signal's angle distribution with collimation optics or an aperture. Computationally efficient algorithms were applied to reduce the number of encoders needed and the chip area of the spectrometer without significantly sacrificing the spectral reconstruction performance. The result is an ultrathin-film form factor, as illustrated in Figure 1, which is suitable for integrating a lab-on-a-chip sensor for epidermal sensors, biochips, neuro- and endoscopic probes, Internet-of-things, and environmental monitoring.

RESULTS

A proof-of-concept chip-scale reconstructive spectrometer consisting of 16 spectral encoders was prepared (Figure 2A; see the Sample Preparation section). Each encoder consisted of a pn junction and therefore also functioned as a photodetector biased at a zero voltage. Moreover, each encoder exhibited a unique spectral responsivity determined by the geometric shape of the constituent light absorbers. The encoder comprises an array of nanopillar-shaped GaN nanostructural light absorbers. The strain profile of the InGaN/GaN multiple quantum wells (MQWs) inside each nanopillar follows a hyperbolic secant (*hsec*) profile along its radial direction with a zero strain (fully relaxed) at the perimeter and an increasing strain (partially relaxed) toward the center.[24] When the nanopillar diameter is large, the strain at the center reaches its maximum value as determined by the lattice mismatch between InGaN and GaN. However, as the nanopillar diameter is on the order of several hundreds of nanometers or smaller, the strain at the center does not reach the maximum value. A smaller strain increases the bandgap and decreases the absorption cutoff wavelength, allowing the spectral response

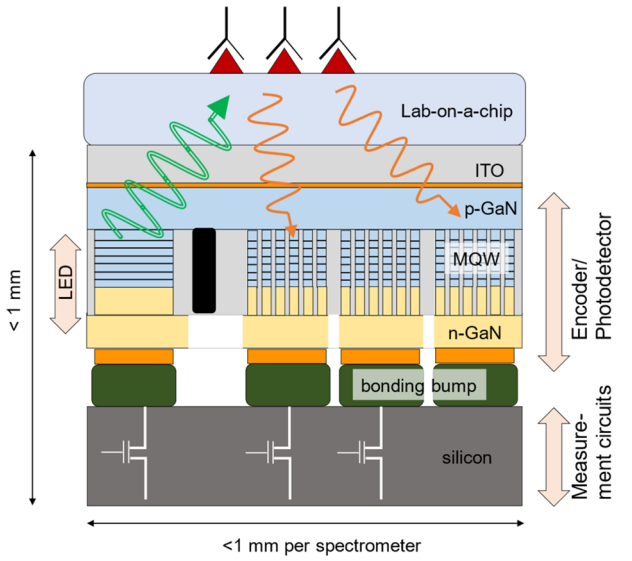

Figure 1. Conceptual illustration of the strategies used to achieve a low-profile ultrathin spectrometer chip based on the spectral reconstruction technique utilizing an array of GaN-based spectral encoders and photodetectors. As shown is the monolithic integration of the GaN reference or excitation LED and three spectral encoders, which double as photodetectors. The programming of each spectral encoder is via local strain engineering using nanopillar-shaped InGaN/GaN multiple quantum wells (MQWs). The weak angle dependence of the spectral encoders' absorption eliminates the need to condition the incident optical signal using collimation optics or apertures, enabling a direct integration on a lab-on-a-chip platform.

to be programmed simply by changing the nanopillar's diameter using lithography and etching. Figure 2B shows the 16 encoders' responsivities $R_k(\lambda)$ measured at 0 V with a 1 nm spectral resolution as a function of the nanopillar's diameter (see the Optical Measurements section). We also determined the operating wavelength range using the NNLS algorithm with a monochromatic delta-function spectrum $\delta(f_0)$ as an input tuned from 400 to 700 nm. We calculated the photocurrents $I_k = R_k\ \delta(f_0)$ and applied NNLS to check how well $\delta(f_0)$ can be recovered. The reconstructed peak wavelength versus the input is plotted in Figure 2C. The straight-line segment from 400 to 645 nm represents the operational window of the device. Beyond 645 nm, the reconstruction error increased significantly because of the low responsivities of all detectors, as shown in Figure 2B. The absorption cutoff wavelength of the MQW stack is around 650 nm.

In a spectrometer, the encoders' spectral responses $R_k(\lambda)$ must remain constant under all measurement conditions for the reconstruction algorithm to determine the spectrum correctly. Thus, the incident light's angle distribution is often conditioned in a reconstructive spectrometer, for example, by letting it go through a pinhole or collimation optics. This is because the spectral response is generally sensitive to the incident angle of light. The external optical elements filter or fix the distribution of the incident angles, but also increase the difficulty of miniaturizing the spectrometer, especially achieving a chip-scale device with a low profile. While an on-chip aperture or a grating coupler has been reported to address this limitation, these structures inevitably reduce the light-harvesting efficiency (LHE) and the signal-to-noise ratio (SNR). Alternatively, a nanostructural absorber can reduce the

https://doi.org/10.1021/acs.nanolett.2c02654
Nano Lett. 2022, 22, 8174−8180

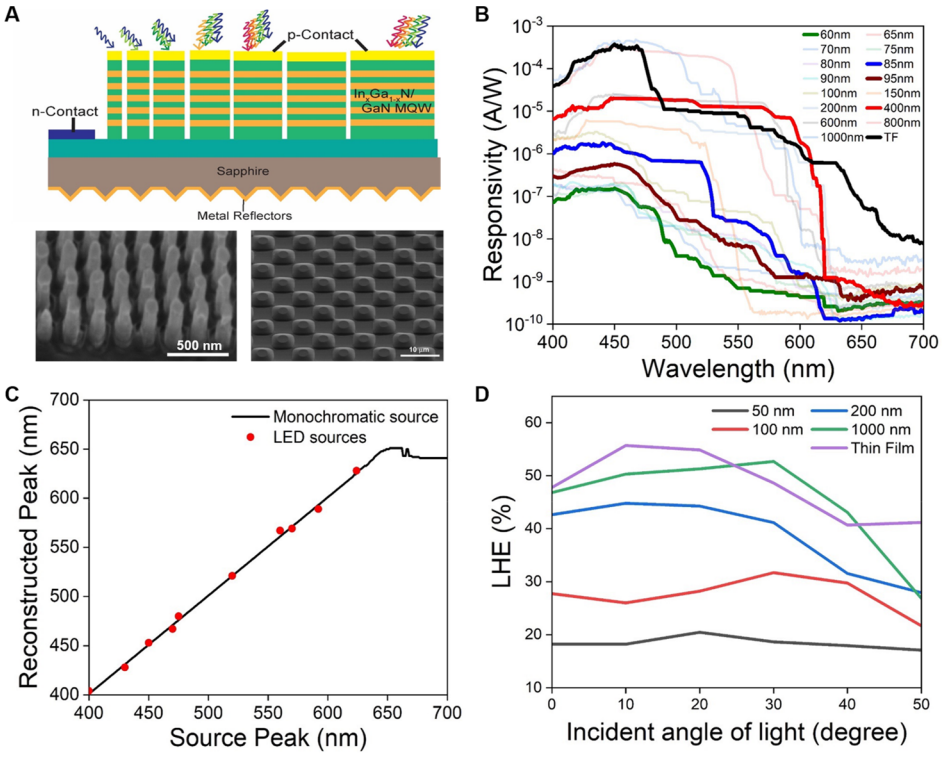

Figure 2. (A) The device schematic shows the cross-sectional view of seven photodetector sections and the light-trapping back reflector on the underside of the sapphire substrate. Each photodetector section consists of a different diameter array of nanopillar-shaped LEDs, which programs the spectral response via local strain engineering. A representative nanopillar array's scanning electron microscopy (SEM) image is shown on the bottom left with the metal etch mask on top of the nanopillars. The etch mask was still needed for the subsequent fabrication process and therefore was not removed for the imaging. The SEM bird's-eye view of the light-trapping back reflector is shown on the bottom right. (B) The responsivities of the 16 photodetectors were measured using a tunable monochromatic light (see the Optical Measurements section). The legend shows the diameter of the nanopillar in each photodetector, ranging from 60 nm to thin film (TF). The responsivity is not normalized to the active region area but rather the chip area. (C) The spectrometer's spectral reconstruction accuracy in the range of 400 to 700 nm, using both the monochromatic input (solid curve) and LED sources (dots). A diagonal section between 400 and 645 nm represents the spectrometer's operating range. (D) The light-harvesting efficiencies (LHEs) of different photodetectors as a function of the incident angle of light are calculated using the three-dimensional finite-difference-time-domain (FDTD) method. The legend shows the diameter of the nanopillar in each photodetector. A bottom light-trapping structure with a sidewall angle of 32°, as shown in (A) was included in the calculations.

sensitivity as light can bounce around between the nanostructures, effectively randomizing the angle distribution. A light-trapping structure that increases light scattering at all angles also helps. This work added a periodic array of microscale dome-like silver-coated back reflectors on the sapphire substrate's back side. Figure 2D shows the LHEs of different encoders as a function of the incident angle of light. The result suggests that the LHE is relatively insensitive to the incident angle of light up to ±30°, corresponding to a numerical aperture of 0.5. The sensitivity increases when the incident angle is more than 30° for larger-diameter and thin-film photodetectors. Further improvements are possible with a second light scatterer or diffuser added on the top[14] or a microlens to function as a spatial filter.

To characterize the spectral reconstruction performance, various commercial 5 mm LEDs of different colors and their combinations were used as the test light sources. These LEDs were mounted around 5 cm above the sample with no special alignment or external optical elements other than making sure the light from all LED devices hit the photodetector area on the sample. A commercial spectrometer separately measured the LED emission to obtain the ground truth.

When reconstructing the spectrum, as there are only 16 spectral encoders, the linear system specified by $R_k(\lambda)$ is heavily underdetermined. Moreover, $R_k(\lambda)$ may change for different scenarios. While the LHE of the photodetectors used in this study is relatively insensitive to the incident angle of light up to ±30°, the sensitivity starts to increase at a larger incident angle for large-diameter and thin-film photodetectors, as shown in Figure 2D. The change of the illumination angle distribution may lead to the uncertainty of $R_k(\lambda)$, which means the reconstructed solution may be inaccurate.

To address both challenges, we introduced a variant of total-variation (TV) regularization.[25] The TV loss is defined as $\|S\|_{\mathrm{TV}}^2 = \frac{1}{2}\|DS\|_2^2$, where $D \in \boldsymbol{R}^{300\times300}$ is the first-order difference matrix given by

$$D = \begin{bmatrix} 1 & -1 & 0 & 0 & 0 & 0 \\ 0 & 1 & -1 & \ddots & \ddots & 0 \\ 0 & 0 & 1 & \ddots & \ddots & 0 \\ 0 & \ddots & \ddots & \ddots & \ddots & 0 \\ 0 & \ddots & \ddots & \ddots & \ddots & -1 \\ 0 & 0 & 0 & 0 & 0 & 1 \end{bmatrix}$$

We solved $\hat{S} = \arg\min_{S\geq 0} \frac{1}{2}\|I - RS\|_2^2 + \lambda\|S\|_{\mathrm{TV}}^2$, where $\lambda > 0$ is the weight of the TV loss. We can interpret the optimization problem as

https://doi.org/10.1021/acs.nanolett.2c02654
Nano Lett. 2022, 22, 8174−8180

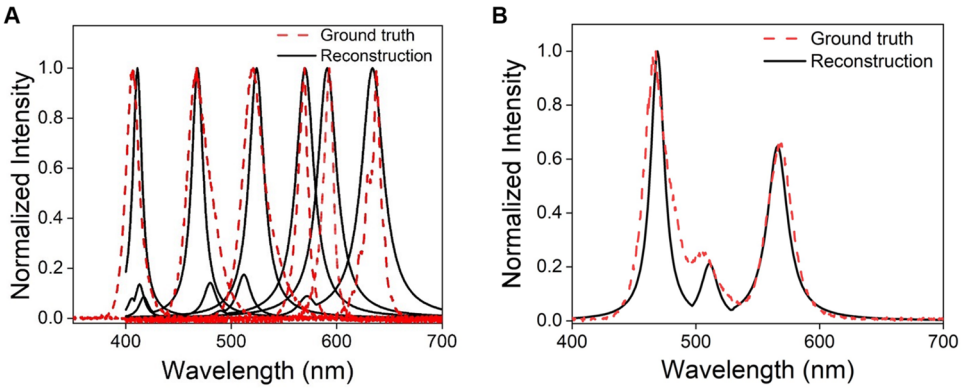

Figure 3. Measured spectra were constructed from a TV-regularized NNLS algorithm (solid curves), and their comparison to the ground truths (dashed curves) measured by a commercial spectrometer. (A) A series of single-color 5 mm LEDs as the test light sources. A total of 10 were measured, with six results shown here (see Supporting Information for the entire data set). (B) Test light source with three 5 mm LEDs of different colors.

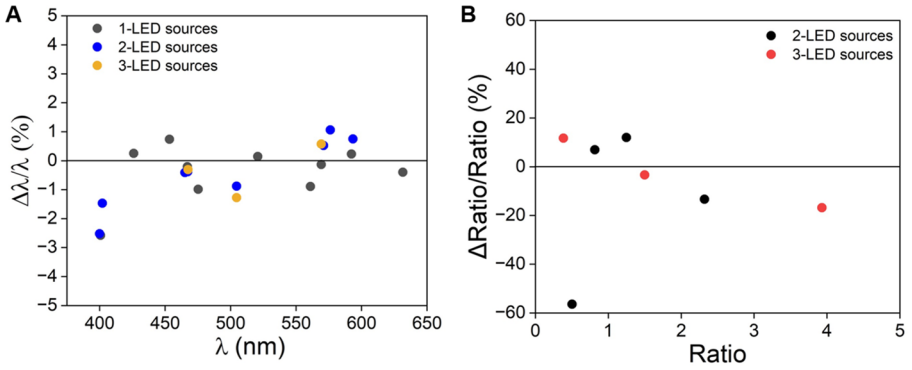

Figure 4. Accuracies of spectral reconstruction performance of various test light sources comprising of 1, 2, and 3 LEDs of different colors. (A) The accuracy of the reconstructed peak wavelength positions $\Delta\lambda = \lambda_{\text{reconstructed}} - \lambda$ as compared to the ground truth (λ). (B) The accuracy of the intensity ratios ΔRatio at different peak wavelengths as compared to the ground truth (Ratio).

$$\hat{S} = \arg\min_{S\geq 0} \frac{1}{2}\left\| \begin{bmatrix} R \\ \lambda D \end{bmatrix} S - \begin{bmatrix} I \\ 0 \end{bmatrix} \right\|_2^2$$

Given the size of the new sensing matrix $\begin{bmatrix} R \\ \lambda D \end{bmatrix}$, the original problem is now transformed into an overdetermined system. This guarantees the uniqueness of our solution for estimating the spectrum. Second, using the modified TV regularizer improves robustness to the uncertainty of $R_k(\lambda)$. It is well understood that adding a regularizing term (e.g., ridge regularization) reduces the sensitivity of the solution $\hat{S}$ to errors in the measurement process.[26] In particular, regularization schemes such as ridge regression are known to be optimally robust against perturbations in the sensing matrix R, which is precisely where the uncertainty arises.[27] Finally, it is worth mentioning that our formulation is a specific instance of generalized ridge regression; in this case, we encourage the reconstructed spectrum to be smooth, which is true for most optical signals.

In the following, we present the results of TV regularized spectral reconstruction with an empirical choice of $\lambda = 10^{-5}$ using MATLAB's lsqnonneg solver. The results are summarized in Figure 3, where Figures 3A and B show the results from a single LED and three LEDs, respectively. More results can be found in the Supporting Information. For many potential applications of a miniaturized spectrometer, the nature of the optical signal is almost always known a priori. In this study, the LED emission can be represented by the sum of multiple Lorentzian-shaped lines, that is, inhomogeneously broadened. Therefore, in addition to the above results from TV regularization, we convolve the result with a Lorentzian kernel function

$$L(\lambda = hc/E,\ \Delta E) = \frac{1}{\pi}\frac{\Delta E/2}{(E - E_0)^2 + \left(\frac{\Delta E}{2}\right)^2}$$

where ΔE is the fwhm line width, h is the Planck's constant, and c is the speed of light. A commercial LED typically has a line width in the range of $3-10kT$. In this work, we chose $\Delta E = 6kT$.

Figure 4 summarizes the spectral reconstruction performance. We focus on the major features of the spectrum, such as the peak positions and the relative optical powers between these peaks, which are likely sufficient for many miniaturized spectrometers' targeted applications. The accuracy of the peak wavelengths has a standard deviation of 0.97%, corresponding to 4 to 6 nm of wavelength accuracy in the visible wavelength range. The accuracy for the intensity ratio at different peak positions is not as good, with a standard deviation of 21.1% (or 10.4% if one outlier is removed). Accurately determining the intensity ratio requires more spectral information and hence a larger number of spectral encoders, which is left for future investigations. Increasing the number of spectral encoders is also expected to improve the wavelength accuracy but at the

https://doi.org/10.1021/acs.nanolett.2c02654
Nano Lett. 2022, 22, 8174−8180

expense of a larger chip area and more computational resources.

DISCUSSION

In this work, we assumed the nature of the optical signal was known to improve the spectral reconstruction with an appropriate kernel. It is likely true that the optical signal in many scenarios is categorizable based on the specific application. On the other hand, those applications often have constraints on system size, thickness, weight, power consumption, and reliability under a constant motion. The proposed spectrometer design in this study is most suitable for applications that prioritize the thinness and lower power consumption over the ability to analyze an arbitrary spectrum with a high spectral resolution. Examples include a wearable or epidermal sensor that regularly monitors an optical signal for a long time.[28−30] By thinning or removing the sapphire substrate and vertically stacking a silicon ASIC that incorporates TIA and microprocessor for spectral reconstruction, as illustrated in Figure 1, the overall dimensions of the spectrometer can be no more than a few hundred micrometers in thickness and a few millimeters in the lateral directions. Multiple photodetectors can share one TIA in a round-robin fashion.

A total of 16 encoders were used in this work. In cases when the number of spectral features is small, it is interesting to ask what the minimum number of spectral encoders is required. To answer this question, we applied a "greedy" algorithm to the 3-LED spectrum. We evaluated a loss function L:

$$L = \sum (x_i - \hat{x}_i)^2 + (p_i - \hat{p}_i)^2$$

where $\{x_i, p_i\}$ are the position and magnitude of the i-th peak of the reconstructed spectrum and $\{\hat{x}_i, \hat{p}_i\}$ are the same for the ground truth. We started with 16 encoders and calculated L by removing one encoder at each iteration. At the end of each iteration, we eliminated the encoder that minimized L for the rest of the encoders. The result is shown in Figure S5. It suggests that the reconstruction of the 3-LED spectrum only requires 7 encoders.

While advanced machine learning methods such as deep learning can likely improve the spectral reconstruction performance, they require training with many test light sources and are time-consuming.[17,20] In this study, an alternative was suggested based on the known nature of the optical signal, in our case, the Lorentzian line shape of the LED emission. Convolving the appropriate kernel with the reconstructed spectrum obtained from a simple NNLS algorithm can significantly increase the computational efficiency of the spectrometer while still achieving a reasonable accuracy. Such an approach can potentially greatly reduce power consumption, a feature likely important for wearable applications.

CONCLUSION

A wafer-thin chip-scale portable spectrometer system based on the NNLS spectral reconstruction algorithm was proposed and demonstrated. A total of 16 spectral encoders, which simultaneously functioned as photodetectors, were monolithically integrated on a chip area of 0.16 mm^2 using the principle of local strain engineering in compressively strained InGaN/GaN MQW structures. When the InGaN MQW active region is shaped into an array of nanopillars, the strain is relaxed from the edge of the nanopillar, which modifies the absorption cutoff wavelength and the spectral response. The absorption properties were programmed and tuned across the visible spectrum using different nanopillar diameters. The built-in GaN pn junction enabled photocurrent measurements at a zero bias. The absorption sensitivity was suppressed for an incident angle of light up to 30° using a cone-shaped back reflector fabricated on the underside of the sapphire substrate. As a result, no external optics such as collimation optics and apertures were used or necessary in the experimental demonstration. A non-negative least-squares (NNLS) algorithm with total-variation (TV) regularization and a choice of Lorentzian kernel function was shown to deliver a decent spectral reconstruction performance in the wavelength range of 400−645 nm. The accuracies of spectral peak positions and intensity ratios between peaks were found to be 0.97% and 10.4%, respectively. The small chip area together with a computationally efficient spectral reconstruction algorithm makes the proposed spectrometer especially suitable for wearable applications.

METHODS

Sample Preparation. The sample used in this study was grown on a 50 mm diameter double-side-polished (DSP), c-plane sapphire substrate by a commercial foundry (NovaGaN) using metal−organic chemical vapor deposition (MOCVD). The epitaxial structure was a simple LED heterostructure with GaN pn junction and five periods of $In_{0.32}Ga_{0.68}N$ (2.5 nm)/GaN (12 nm) multiple quantum wells (MQWs) in the active region. No electron blocking layer was added. The indium composition in the MQWs was controlled such that electroluminescence at room temperature showed red emission (λ = 630 nm at 7 V). The sample fabrication (see Supporting Information, Figure S4) started with the underside of the substrate with the preparation of dome-like light trapping structures. First, 500 nm thick SiO_2 was deposited on the front side of the substrate to protect the epilayers. A photoresist (SPR 220) was then spin-coated on the back side of the substrate and patterned with an array of circles (4 μm diameter with an interval of 3 μm) using optical lithography. The resist was reflowed at 140 °C for 6 min using a hot plate in air to achieve the desired shape. Next, the resist pattern was transferred to the sapphire substrate using inductively coupled-plasma-reactive-ion-etching (ICP-RIE), resulting a sidewall angle of ∼32°. The shape and sidewall angles of the dome-structures were verified by atomic force microscopy. After ICP-RIE, SiO_2 layer was removed using buffered HF. A 300 nm thick Ag layer was deposited on the domes as the reflector. The scanning electron microscopy (SEM) image of the backreflector is also shown in Figure 2A.

The photodetectors with integrated spectral encoders were fabricated by a top-down process. Electron beam lithography and ICP-RIE were used to define the nanopillars of various diameters. To get a vertical sidewall and remove the plasma damage, a wet etch in a buffered KOH solution (AZ 400 K) was performed after the dry etch. The SEM image for the 60 nm GaN nanopillars is shown in Figure 2A. After achieving cylindrical nanopillars with a height of 200 nm, the sample was planarized. A 500 nm SiO_2 was deposited using plasma-enhanced chemical vapor deposition (PECVD) followed by a 600 nm spin coating of poly(methyl methacrylate) (PMMA). After planarization, PMMA and SiO_2 were etched back using ICP-RIE with a subsequent ion milling to expose the tips of the nanopillars. Ion milling was used to avoid the plasma damage

https://doi.org/10.1021/acs.nanolett.2c02654
Nano Lett. 2022, 22, 8174−8180

on the circumference of the exposed nanopillars. Finally, the metallization for the electrical interconnects was carried out. We used 7 nm/7 nm Ni/Au layer for p-contact thermally annealed in air and 30 nm/100 nm Ti/Au for n-contact. All photodiodes share a common n-contact.

Optical Measurements. Each photodiode was characterized for its intrinsic response under the illumination of a monochromatic light in the spectral range of 400 to 700 nm with a step size of 1 nm. We used a solar simulator (Abet Technologies) as the light source. The broadband spectrum was filtered through a monochromator (Acton 2500i, 0.500m focal length triple-grating) and impinged upon each photodiode via fiber optic cable. The photocurrent was measured at 0 V using a current meter (Keithley 6482). The optical power of the impinged light was separately measured from a reference detector. The responsivity of each photodiode was calculated from the measured photocurrent and optical power of incident light. We also considered the estimated illumination area and the dimensions of each photodiode (including areas without nanopillars) in the responsivity calculations.

■ ASSOCIATED CONTENT

Supporting Information

The Supporting Information is available free of charge at https://pubs.acs.org/doi/10.1021/acs.nanolett.2c02654.

Additional experimental data of different test light sources; Detailed sample fabrication flow (PDF)

■ AUTHOR INFORMATION

Corresponding Author

Pei-Cheng Ku − *Department of Electrical Engineering and Computer Science, University of Michigan, Ann Arbor, Michigan 48109-2122, United States;* orcid.org/0000-0003-2282-5954; Email: peicheng@umich.edu

Authors

Tuba Sarwar − *Department of Electrical Engineering and Computer Science, University of Michigan, Ann Arbor, Michigan 48109-2122, United States*

Can Yaras − *Department of Electrical Engineering and Computer Science, University of Michigan, Ann Arbor, Michigan 48109-2122, United States*

Xiang Li − *Department of Electrical Engineering and Computer Science, University of Michigan, Ann Arbor, Michigan 48109-2122, United States*

Qing Qu − *Department of Electrical Engineering and Computer Science, University of Michigan, Ann Arbor, Michigan 48109-2122, United States*

Complete contact information is available at: https://pubs.acs.org/10.1021/acs.nanolett.2c02654

Author Contributions

P.C.K. and Q.Q. conceived the concepts of the spectrometer design and spectral reconstruction, respectively. T.S. prepared the sample and performed the optical measurements. P.C.K. and T.S. analyzed and interpreted the experimental data. C.Y. and X.L. carried out spectral reconstruction under the supervision of Q.Q.

Funding

This work was primarily supported by the University of Michigan ESSI, the University of Michigan Blue Sky Initiative (for the sample design, fabrication, and measurements), and the University of Michigan MIDAS PODS Grant. Q.Q. also acknowledges supports from the National Science Foundation under the Award No. CAREER 2143904, CCF 2212066, and the Office of Naval Research under the Award No. N00014-22-1-2529.

Notes

The authors declare no competing financial interest.

■ REFERENCES

(1) Shafer, A. B.; Megill, L. R.; Droppleman, L. Optimization of the Czerny−Turner Spectrometer*. *J. Opt. Soc. Am.* **1964**, *54* (7), 879−887.

(2) Khan, Y.; Han, D.; Pierre, A.; Ting, J.; Wang, X.; Lochner, C. M.; Bovo, G.; Yaacobi-Gross, N.; Newsome, C.; Wilson, R.; Arias, A. C. A Flexible Organic Reflectance Oximeter Array. *Proc. Natl. Acad. Sci. U. S. A.* **2018**, *115* (47), E11015−E11024.

(3) Stojanovic, R.; Karadaglic, D. Design of an Oximeter Based on LED-LED Configuration and FPGA Technology. *Sensors (Switzerland)* **2013**, *13* (1), 574−586.

(4) Candès, E. J.; Romberg, J.; Tao, T. Robust Uncertainty Principles: Exact Signal Reconstruction from Highly Incomplete Frequency Information. *IEEE Trans. Inf. Theory* **2006**, *52* (2), 489−509.

(5) Bao, J.; Bawendi, M. G. A Colloidal Quantum Dot Spectrometer. *Nature* **2015**, *523* (7558), 67−70.

(6) Guyot-Sionnest, P.; Ackerman, M. M.; Tang, X. Colloidal Quantum Dots for Infrared Detection beyond Silicon. *J. Chem. Phys.* **2019**, *151* (6), 060901.

(7) Wang, Z.; Yu, Z. Spectral Analysis Based on Compressive Sensing in Nanophotonic Structures. *Opt. Express* **2014**, *22* (21), 25608.

(8) Hu, X.; Liu, H.; Wang, X.; Zhang, X.; Shan, Z.; Zheng, W.; Li, H.; Wang, X.; Zhu, X.; Jiang, Y.; Zhang, Q.; Zhuang, X.; Pan, A. Wavelength Selective Photodetectors Integrated on a Single Composition-Graded Semiconductor Nanowire. *Adv. Opt. Mater.* **2018**, *6* (12), 1800293.

(9) Wang, Z.; Yi, S.; Chen, A.; Zhou, M.; Luk, T. S.; James, A.; Nogan, J.; Ross, W.; Joe, G.; Shahsafi, A.; Wang, K. X.; Kats, M. A.; Yu, Z. Single-Shot on-Chip Spectral Sensors Based on Photonic Crystal Slabs. *Nat. Commun.* **2019**, *10* (1), 1020.

(10) Yang, Z.; Albrow-Owen, T.; Cui, H.; Alexander-Webber, J.; Gu, F.; Wang, X.; Wu, T. C.; Zhuge, M.; Williams, C.; Wang, P.; Zayats, A. V.; Cai, W.; Dai, L.; Hofmann, S.; Overend, M.; Tong, L.; Yang, Q.; Sun, Z.; Hasan, T. Single-Nanowire Spectrometers. *Science* **2019**, *365* (6457), 1017−1020.

(11) Laux, E.; Genet, C.; Skauli, T.; Ebbesen, T. W. Plasmonic Photon Sorters for Spectral and Polarimetric Imaging. *Nat. Photonics* **2008**, *2* (3), 161−164.

(12) Park, H.; Dan, Y.; Seo, K.; Yu, Y. J.; Duane, P. K.; Wober, M.; Crozier, K. B. Filter-Free Image Sensor Pixels Comprising Silicon Nanowires with Selective Color Absorption. *Nano Lett.* **2014**, *14* (4), 1804−1809.

(13) Sarwar, T.; Cheekati, S.; Chung, K.; Ku, P.-C. On-Chip Optical Spectrometer Based on GaN Wavelength-Selective Nanostructural Absorbers. *Appl. Phys. Lett.* **2020**, *116* (8), 081103.

(14) Kim, J.; Cheekati, S.; Sarwar, T.; Ku, P. Designing an Ultrathin Film Spectrometer Based on III-Nitride Light-Absorbing Nanostructures. *Micromachines* **2021**, *12* (7), 760.

(15) Kim, C.; Lee, W.-B.; Lee, S. K.; Lee, Y. T.; Lee, H.-N. Fabrication of 2D Thin-Film Filter-Array for Compressive Sensing Spectroscopy. *Opt. Lasers Eng.* **2019**, *115*, 53−58.

(16) Kurokawa, U.; Choi, B. Il; Chang, C.-C. Filter-Based Miniature Spectrometers: Spectrum Reconstruction Using Adaptive Regularization. *IEEE Sens. J.* **2011**, *11* (7), 1556−1563.

(17) Brown, C.; Goncharov, A.; Ballard, Z. S.; Fordham, M.; Clemens, A.; Qiu, Y.; Rivenson, Y.; Ozcan, A. Neural Network-Based On-Chip Spectroscopy Using a Scalable Plasmonic Encoder. *ACS Nano* **2021**, *15* (4), 6305−6315.

(18) Xiong, J.; Cai, X.; Cui, K.; Huang, Y.; Yang, J.; Zhu, H.; Li, W.; Hong, B.; Rao, S.; Zheng, Z.; Xu, S.; He, Y.; Liu, F.; Feng, X.; Zhang, W. Dynamic Brain Spectrum Acquired by a Real-Time Ultraspectral Imaging Chip with Reconfigurable Metasurfaces. *Optica* **2022**, *9* (5), 461.
(19) Zhang, S.; Dong, Y.; Fu, H.; Huang, S.-L.; Zhang, L. A Spectral Reconstruction Algorithm of Miniature Spectrometer Based on Sparse Optimization and Dictionary Learning. *Sensors* **2018**, *18* (2), 644.
(20) Meng, J.; Cadusch, J. J.; Crozier, K. B. Plasmonic Mid-Infrared Filter Array-Detector Array Chemical Classifier Based on Machine Learning. *ACS Photonics* **2021**, *8* (2), 648−657.
(21) Sarwar, T.; Ku, P. C. Ultrathin Optics-Free Spectrometer with Monolithically Integrated LED Excitation. *Micromachines* **2022**, *13* (3), 382.
(22) Padmanabhan, P.; Hancock, B.; Nikzad, S.; Bell, L. D.; Kroep, K.; Charbon, E. A Hybrid Readout Solution for GaN-Based Detectors Using CMOS Technology. *Sensors (Switzerland)* **2018**, *18* (2), 449.
(23) Pandey, V. K.; Tan, C. M. Application of Gallium Nitride Technology in Particle Therapy Imaging. *IEEE Trans. Nucl. Sci.* **2021**, *68* (6), 1319−1324.
(24) Zhang, L.; Lee, L.-K.; Teng, C.-H.; Hill, T. A.; Ku, P.-C.; Deng, H. How Much Better Are InGaN/GaN Nanodisks than Quantum Wells—Oscillator Strength Enhancement and Changes in Optical Properties. *Appl. Phys. Lett.* **2014**, *104* (5), 051116.
(25) Rudin, L. I.; Osher, S.; Fatemi, E. Nonlinear Total Variation Based Noise Removal Algorithms. *Phys. D Nonlinear Phenom.* **1992**, *60* (1−4), 259−268.
(26) Tikhonov, A. N.; Arsenin, V. Y. Solutions of Ill-Posed Problems. *SIAM Rev.* **1979**, *21* (2), 266−267.
(27) Bertsimas, D.; Copenhaver, M. S. Characterization of the Equivalence of Robustification and Regularization in Linear and Matrix Regression. *Eur. J. Oper. Res.* **2018**, *270* (3), 931−942.
(28) Zhang, Q.; Wang, X.; Decker, V.; Meyerhoff, M. E. Plasticizer-Free Thin-Film Sodium-Selective Optodes Inkjet-Printed on Transparent Plastic for Sweat Analysis. *ACS Appl. Mater. Interfaces* **2020**, *12* (23), 25616−25624.
(29) Choi, J.; Bandodkar, A. J.; Reeder, J. T.; Ray, T. R.; Turnquist, A.; Kim, S. B.; Nyberg, N.; Hourlier-Fargette, A.; Model, J. B.; Aranyosi, A. J.; Xu, S.; Ghaffari, R.; Rogers, J. A. Soft, Skin-Integrated Multifunctional Microfluidic Systems for Accurate Colorimetric Analysis of Sweat Biomarkers and Temperature. *ACS Sensors* **2019**, *4* (2), 379−388.
(30) Choi, J.; Ghaffari, R.; Baker, L. B.; Rogers, J. A. Skin-Interfaced Systems for Sweat Collection and Analytics. *Sci. Adv.* **2018**, *4* (2), eaar3921.

https://doi.org/10.1021/acs.nanolett.2c02654
Nano Lett. 2022, 22, 8174−8180